Supporting Information

Technical Note: Pyrolysis principles explain time-resolved organic aerosol release from biomass burning

Mariam Fawaz, Anita Avery, Leah R. Williams, Timothy B. Onasch, Tami C. Bond

Number of figures: 40
Number of tables: 1
Number of pages: 27

Supporting information sections:
S1. Experimental Method Supporting Details
S2. EEPS Size Correction
S3. EEPS and DustTrak Comparison
S4. Supporting Figures for Results Section

S1 Experimental Method Supporting Details

Figure S1. The end grain and long grain of the wood types used in the experiments

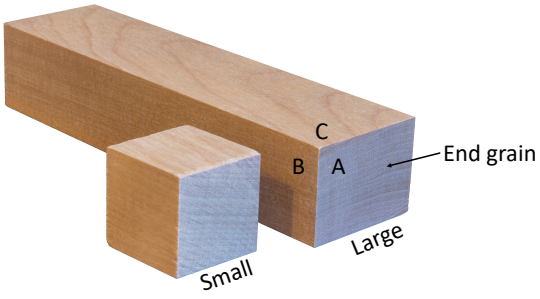

Figure S2. Small and large wood samples with labels corresponding to: (A) small face side view (end grain), (B) long face side view, and (C) top view (long grain)

Table S1. Conditions of the replicated experiments and reported in the manuscript

Experiment Number	Wood Type	Temperature (°C)	Wood Mass (g)	Wood Size (cm)	Secondary Dilution Ratio
77	Birch	600	108	14x3.8x2.9	109
78	Birch	600	106	14x3.8x2.9	213
54	Birch	500	110	14x3.8x2.9	170
55	Birch	500	106	14x3.8x2.9	177
56	Birch	400	104	14x3.8x2.9	195
57	Birch	400	105	14x3.8x2.9	195
138	PineR	600	79	14x3.8x2.9	168
139	PineR	600	78	14x3.8x2.9	178
140	PineR	500	78	14x3.8x2.9	183
141	PineR	500	79	14x3.8x2.9	183
142	PineR	400	78	14x3.8x2.9	183
143	PineR	400	79	14x3.8x2.9	180
177	PineR	600	10.9	2.9x2.9x2.9	160
178	PineR	600	11.1	2.9x2.9x2.9	156
179	PineR	500	11.3	2.9x2.9x2.9	170
180	PineR	500	11	2.9x2.9x2.9	174
181	PineR	400	11.6	2.9x2.9x2.9	160
182	PineR	400	12.7	2.9x2.9x2.9	156
216	Birch	600	14.2	2.9x2.9x2.9	170
217	Birch	600	14.8	2.9x2.9x2.9	169
218	Birch	500	14.7	2.9x2.9x2.9	168
219	Birch	500	14.4	2.9x2.9x2.9	173
220	Birch	400	14.7	2.9x2.9x2.9	168
221	Birch	400	14.7	2.9x2.9x2.9	168
190	Wet PineR	600	74	14x3.8x2.9	192
191	Wet PineR	600	73	14x3.8x2.9	197
192	Wet PineR	500	73	14x3.8x2.9	197
193	Wet PineR	500	80	14x3.8x2.9	180
194	Wet PineR	400	78	14x3.8x2.9	180
195	Wet PineR	400	80	14x3.8x2.9	180
210	PineE	600	81	14x3.8x2.9	160
211	PineE	600	85	14x3.8x2.9	174
212	PineE	500	82	14x3.8x2.9	189
213	PineE	500	85	14x3.8x2.9	178
214	PineE	400	82	14x3.8x2.9	169
215	PineE	400	82	14x3.8x2.9	173
165	Poplar	600	88	14x3.8x2.9	182
166	Poplar	600	87	14x3.8x2.9	190
167	Poplar	500	87	14x3.8x2.9	196
168	Poplar	500	88	14x3.8x2.9	196
169	Poplar	400	81	14x3.8x2.9	196
170	Poplar	400	83	14x3.8x2.9	200
151	Douglas fir	600	90	14x3.8x2.9	186
152	Douglas fir	600	92	14x3.8x2.9	166
153	Douglas fir	500	89	14x3.8x2.9	170
154	Douglas fir	500	93	14x3.8x2.9	181
155	Douglas fir	400	90	14x3.8x2.9	186
156	Douglas fir	400	88	14x3.8x2.9	181

Table S1. table continued

Experiment Number	Wood Type	Temperature (°C)	Wood Mass (g)	Wood Size (cm)	Secondary Dilution Ratio
144	Ipe	600	146	14x3.8x2.9	179
145	Ipe	600	142	14x3.8x2.9	196
146	Ipe	500	145	14x3.8x2.9	202
147	Ipe	500	148	14x3.8x2.9	164
148	Ipe	400	143	14x3.8x2.9	173
149	Ipe	400	143	14x3.8x2.9	178
159	Maple	600	113	14x3.8x2.9	196
160	Maple	600	114	14x3.8x2.9	174
161	Maple	500	115	14x3.8x2.9	174
162	Maple	500	115	14x3.8x2.9	179
163	Maple	400	115	14x3.8x2.9	179
164	Maple	400	114	14x3.8x2.9	184

S2 EEPS Size Correction

Multiple references have reported problems with the sizing and counting of aerosol particles while using the Engine Exhaust Particle Sizer (EEPS 3090, TSI) (Zimmerman et al., 2015, 2014; Levin et al., 2015; Wang et al., 2016). We use a correction method for the sizing of particles developed by Lee et al. (2013). The method compares the output of the EEPS to the size distributions from the Long Time of Flight Aerosol Mass Spectrometer (LToF-AMS, Aerodyne Research, Inc.) and finds a correction for the sizing error that arises. Two sets of experiments were performed, the first to find the correction equation using size-selected ammonium nitrate particles and the second to test the derived correction equation using wood pyrolysis emissions. An evaluation of is presented to examine the effect of the size correction on the results.

S2.1 Procedure

S2.1.1 Ammonium nitrate calibration

AMS instruments measure size-resolved chemical composition of aerosols. Aerosol sizing is measured during the particle time of flight (PToF) mode, where the time a particle takes to travel between the chopper and detector are recorded, and with calibration, that time is converted to a particle size (DeCarlo et al., 2004). The size measured by the AMS, the vacuum aerodynamic diameter (D_{va}) is a function of the aerodynamic diameter and particle density, both of which are known in the following experiments of size-selected ammonium nitrate. Therefore, the AMS is used here as an independent sizing measurement for calibrating the EEPS in the method described in Lee et al. (2013).
Figure S3 shows the schematic for the generation and measurement of ammonium nitrate. Ammonium nitrate was atomized in de-ionized water using a constant output atomizer (TSI 3076). The particles were neutralized and an electrostatic classifier (DMA 3071,TSI) selected particle sizes based on the voltage supplied. The monodisperse aerosol flow was split between the EEPS and the AMS.

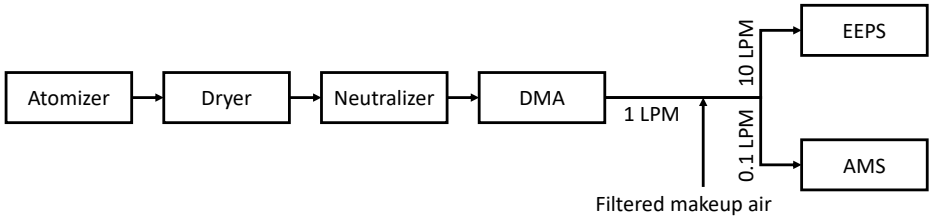

Figure S3. Schematic of the ammonium nitrate calibration experiment between the AMS and EEPS

Ten diameters between 50 nm and 350 nm were selected with the DMA to evaluate the sizing of the EEPS: 56 nm, 69 nm, 194 nm, 247 nm, 278 nm, 293 nm, 305 nm, 322 nm, 341 nm, 344 nm. The experiments focused on these diameters because the size distributions of the particles emitted showed that the mean diameters were greater than 100 nm. Also, it has been reported that the EEPS underestimates the size of particles that have a diameter larger than 90 nm Zimmerman et al. (2015).
Although the EEPS measures from 6-560 nm, the smallest diameter investigated was 56 nm because the AMS has 50% transmission at 60 nm and a lower transmission below that diameter Liu et al. (2007). The AMS collection efficiency (CE) of ammonium nitrate in the calibration is 1, and the AMS CE of the pyrolysis emissions are also likely 1 because they are liquid organics that are unlikely to bounce.

S2.2 Output

Figure S4 shows the comparison of the ten selected diameters for both EEPS and AMS. The EEPS measures number distributions based on the electrical mobility diameter and the AMS measures mass distributions based on the vacuum aerodynamic diameter. The AMS data were converted to number distributions versus mobility diameter using the material density (ρ = 1.72 g/cm^3 for ammonium nitrate) and the Jayne shape factor Jayne et al. (2000). The comparison shows that the EEPS accurately

sizes particles below 100 nm. Based on this data, between 100 nm and 300 nm, the EEPS undersizes the particles and the number concentrations are within the same order of magnitude. Above 300 nm, the EEPS both undersizes and undercounts particles.

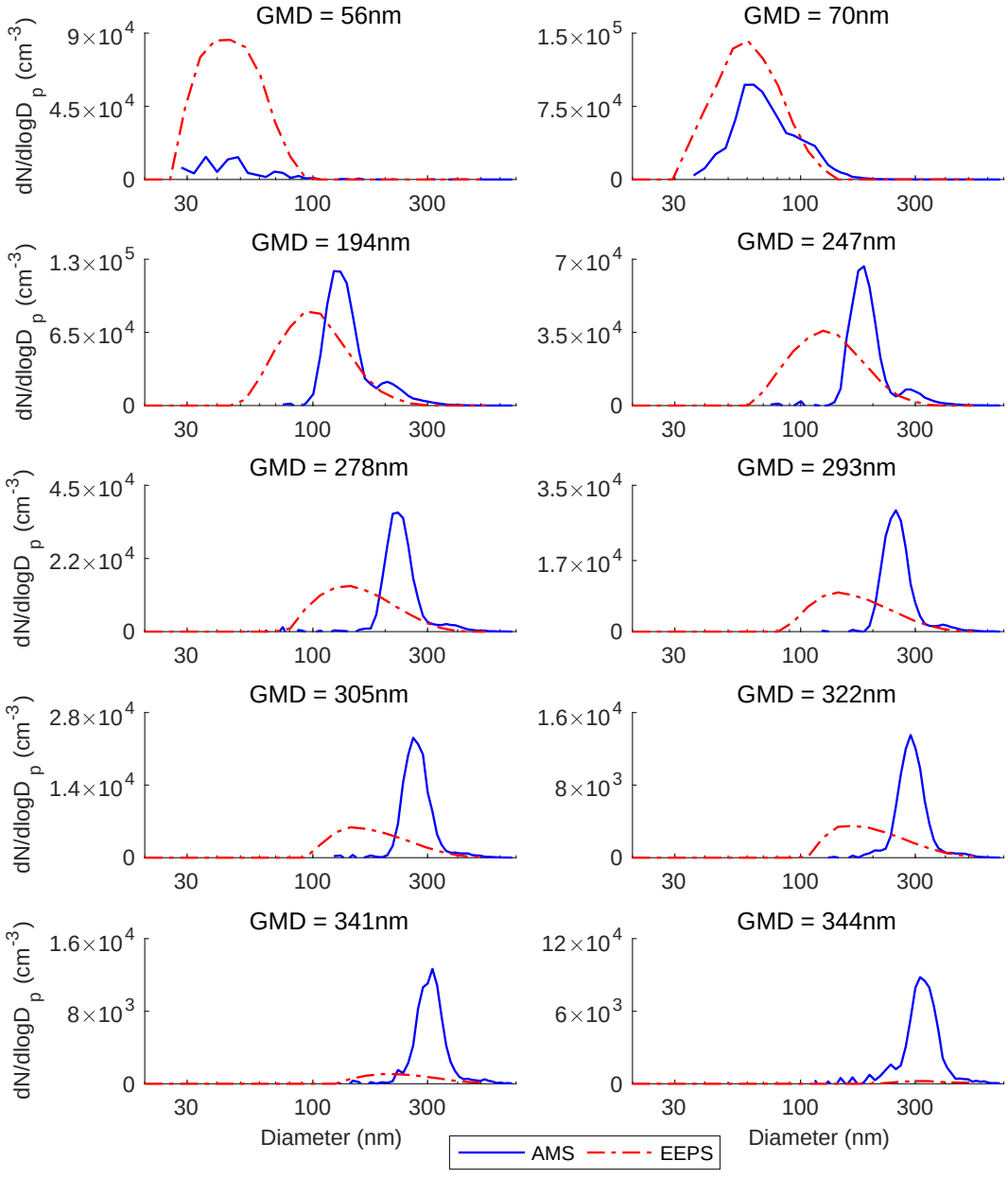

Figure S4. Comparison between number distribution from the EEPS and the AMS using the electrical mobility diameter

S2.3 Data processing

The data outputted from the AMS is D_{va} v. dM/dlogD_p, the vacuum diameter was changed to electrical mobility diameter by using $D_{vac} = D_e \times S \times \rho_p$, the density of ammonium nitrate used ρ_p was 1.72g/cm^3, and the Jayne shape factor S was 0.8. dM/dloD_p was changed to dM. dM was then changed to dN using $\frac{6}{\rho} dM \frac{1}{10^6 \pi D_p^3}$. In the calculations, the double charged particles were removed by identifying the second peak in the mass distribution and subtracting the additional part of the mass distribution from the original mass distribution.

The EEPS uses matrices to change from electrometer current to particle count. The compact matrix that changes from measured current to particle count was used in this analysis to remove double charging by the EEPS Wang et al. (2016).

S2.4 Correction Procedure

Baesd on Lee *et al.* Lee et al. (2013), the geometric mean diameter (GMD) of the AMS was used to correct the diameter of the EEPS as shown in the Figure S5. The fit equation for the change in diameter D_{new} = 1.7*D_{EEPS}-27. The last two data points (D_p = 341 and 344 nm) were removed from the regression because the detection in the EEPS was very low for those two diameters. To avoid negative diameters the first initial diameters before 27 nm were kept from the original scheme. The number distribution is now shifted to the new corrected diameters. The mass size distribution is then calculated based on the new corrected diameters and integrated to yield the mass of the particles.

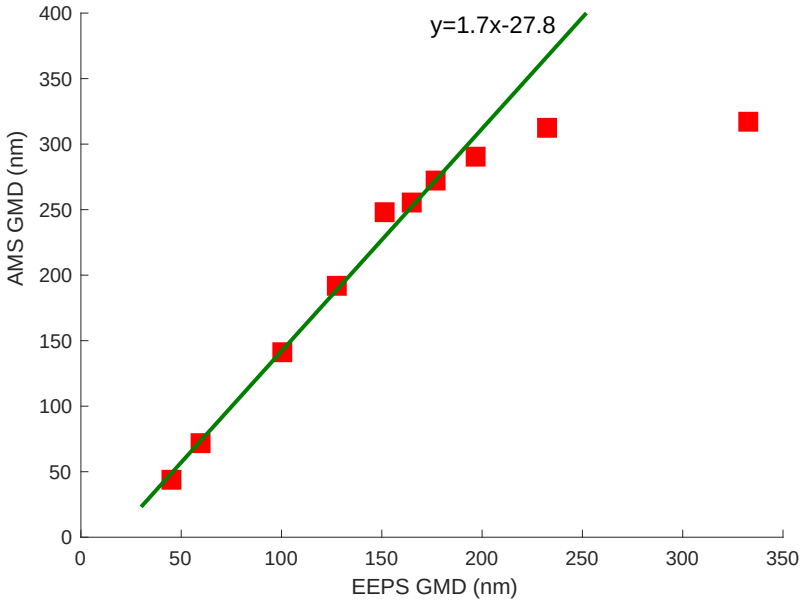

Figure S5. Comparison between number distribution of EEPS and AMS

S2.5 Evaluation

We evaluate the influence of the correction described in this section and applied on the results reported in the paper. In this evaluation, we compare the total mass of the particles measured by AMS and EEPS froma series of pyrolysis experiments and we compare the normalized real-time concentrations of particles before and after correction. The AMS real-time data was not used, because the AMS does not have a good time resolution.

S2.5.1 Particle Yield

An independent data set of pyrolysis experiments were used to evaluate the effect of the correction procedure on the yield of particles. Figure S6 shows the comparison between the particle yield of the AMS and that of the EEPS before and after correction for 12 wood pyrolysis experiments. The original set is the particle yield using EEPS measurements before correction, and the corrected set is the particle yield set using EEPS measurements after correction. The adjusted set of EEPS particle yield was calculated using the corrected diameters. The original set shows that the EEPS measurement error is significantly high, and the corrected set shows a better agreement with the results of the particle yield as measured by the AMS. The sum of square errors (SSE) for the original set was 0.056 and that of the corrected set was 0.0051. The correction achieved an order of magnitude reduction in the SSE between the two sets.

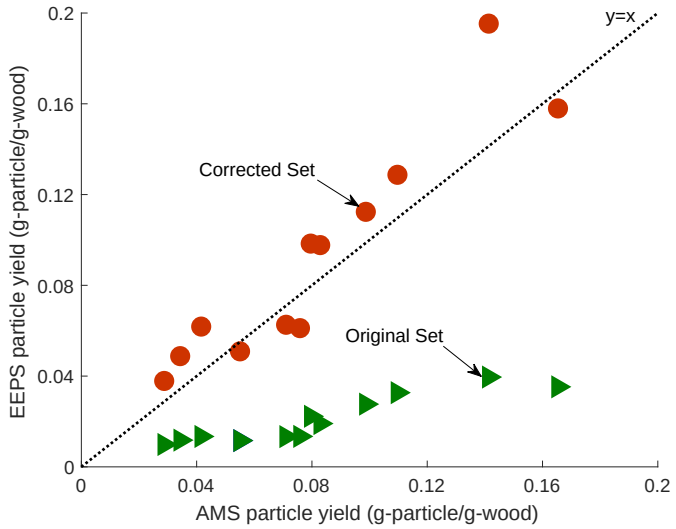

Figure S6. EEPS particle yield versus AMS particle yield, the uncorrected set is in the green triangles and the corrected set for EEPS sizing errors is in the red circles

S2.5.2 Real-time Behavior

The influence of the diameter dependent correction on the real-time behavior was assessed by comparing the particle mass concentration before and after correction. Figure S7 - S8 shows the comparison for birch wood at 500 and 600°C, and Figure S9 - S10 shows the comparison for pineR at 500 and 600°C.

The normalized concentrations in Figures S7 and Figure S9 is the real-time particle mass concentration divided by the maximum concentration measured in the experiment. The real-time concentrations before and after correction are similar, this is further demonstrated in Figures S8 and Figure S10 where the ratio of the normalized concentrations are plotted. The average difference between the two normalized signal at 500°C is within 3% for pineR and birch and at 600°C within 7% for pineR and birch.

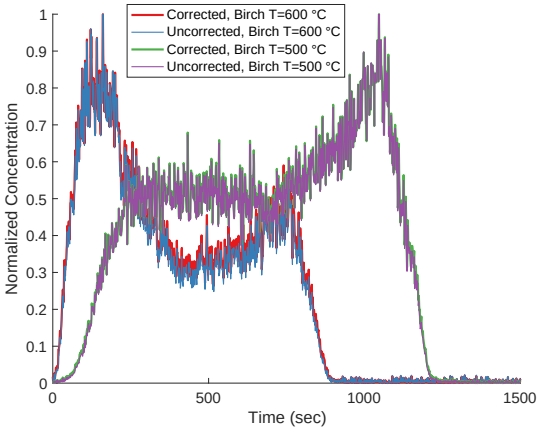

Figure S7. Normalized particle mass concentration for birch pyrolysis experiment at 500 and 600°C

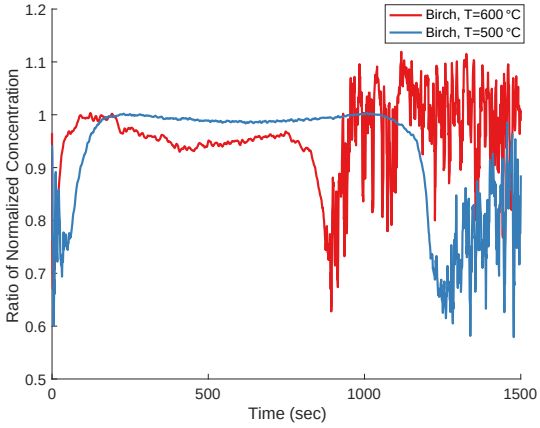

Figure S8. Ratio of the normalized concentration Normalized particle mass concentration for birch pyrolysis experiment at 500 and 600°C

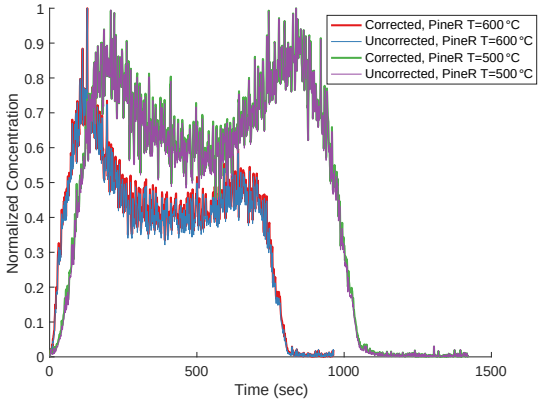

Figure S9. Normalized particle mass concentration for pineR pyrolysis experiment at 500 and 600°C

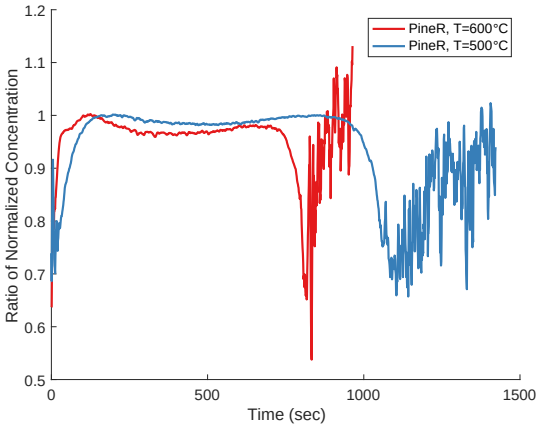

Figure S10. Ratio of the normalized concentration Normalized particle mass concentration for pineR pyrolysis experiment at 500 and 600°C

S2.5.3 Summary

The EEPS have been reported to have measurement errors; there are a limited number of methods in literature that address the error and present comparisons between the EEPS output and another real-time instrument. We compared our measurements to the AMS measurements to estimate the extent of the error and correct for it. After applying a correction method, we evaluated the effect of the correction on the main findings of the paper: (1) the yield of the particles collected in the experiments, (2) the real-time particle mass concentration. The yields from the corrected EEPS data set were very close to those calculated from AMS measurement, and the difference between the normalized real-time concentration from the EEPS before and after correction differed by less than 10%. The real-time concentration behavior was unchanged by the correction preserving the main finding of the work that the particle emission follows the mass loss rate.

S3 EEPS and DustTrak Comparison

The EEPS has a limited size range. At moderate and high reactor temperatures (500 and 600°C), the size distribution of particles emitted can be fully counted by the EEPS. At 400°C the size distribution of the particle emitted extends beyond the detection size range of the EEPS. A DustTrak was connected in parallel to the EEPS, the total mass of the particles from the DustTrak was used in the cases when the EEPS could not measure the entire size distribution. In this section we show the EEPS output and a comparison between the DustTrak and EEPS data at all temperatures for both birch and pineR.

S3.1 EEPS PyOM Output

Figures S12, S13 and S15 show the real-time PyOM concentration for birch and pineR at 400, 500, and 600°C respectively. Figures S11,S14, and S16 show the geometric mean diameter (GMD) for birch and pineR at 400, 500, and 600°C respectively. There is a clear gap in the measurements for birch (Figure S12). Which occurs because the size distribution extends beyond 60nm - 560nm range of the EEPS. The PyOM mass concentration at 400°C as measured by the EEPS does not follow the mass loss rate, and the gases concentrations as observed at 500 and 600°C. We will demonstrate in the next section that the DustTrak shows that the PyOM concentrations follows the other measured quantities at all temperatures.

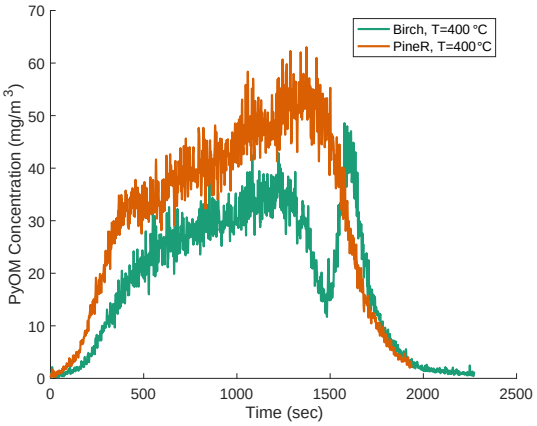

Figure S12. PyOM mass concentration for birch and pineR at 400°C using the size distribution measured by the EEPS

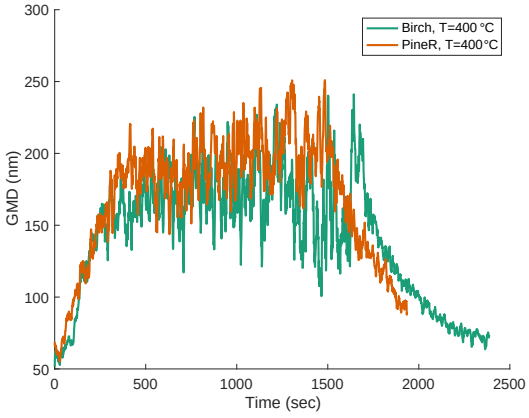

Figure S11. Geometric mean diameter (GMD) for birch and pineR at 400°C using the size distribution measured by the EEPS

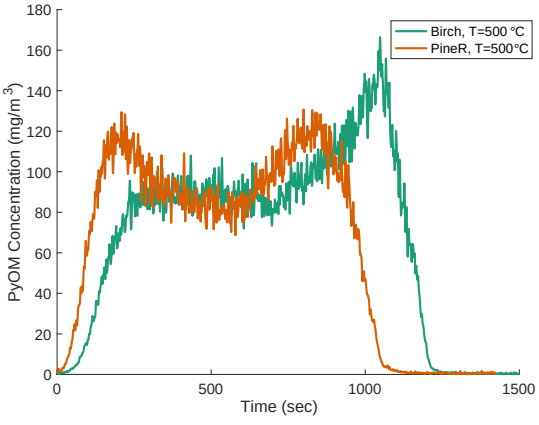

Figure S13. PyOM mass concentration for birch and pineR at 500°C using the size distribution measured by the EEPS

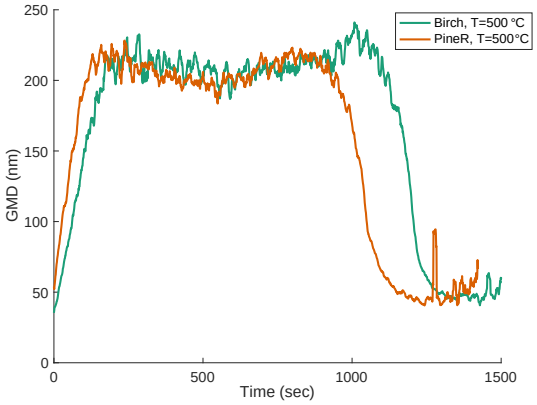

Figure S14. Geometric mean diameter (GMD) for birch and pineR at 500°C using the size distribution measured by the EEPS

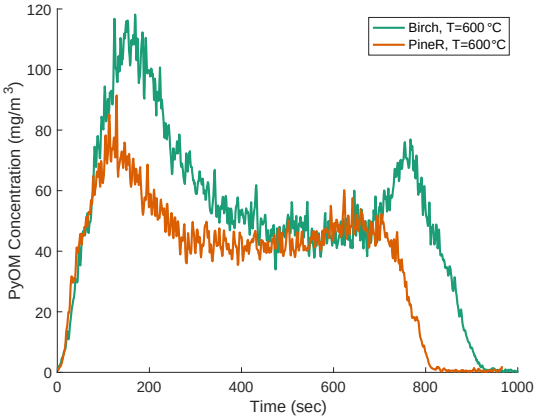

Figure S15. PyOM mass concentration for birch and pineR at 600°C using the size distribution measured by the EEPS

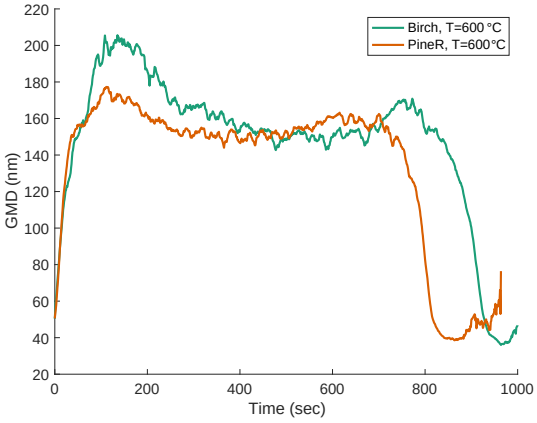

Figure S16. Geometric mean diameter (GMD) for birch and pineR at 600°C using the size distribution measured by the EEPS

S3.2 DustTrak Comparison

Figures S17, S18, S19, and S20 show the comparison between DustTrak measurements for pyrolysis experiments at 400 and 500°C for pineR and birch. At 500°C experiments the Dusttrak and EEPS measurements are similar and there is little difference in the measurements of PyOM concentrations. The real-time behavior as measured by the EEPS and the DustTrak is preserved and the two peaks are observed in both instrument measurements. As measured by the DustTrak, the real-time PyOM concentration follows the mass loss rate of the wood and the real-time gases concentrations at all temperatures.
At 400°C the EEPS does not capture the entire size distribution of the emitted particles. We replace the EEPS measurements with DustTrak measurements only at this reactor temperature. This problem of the missing size distribution is not encountered at 500 and 600°C reactor temperature experiments.

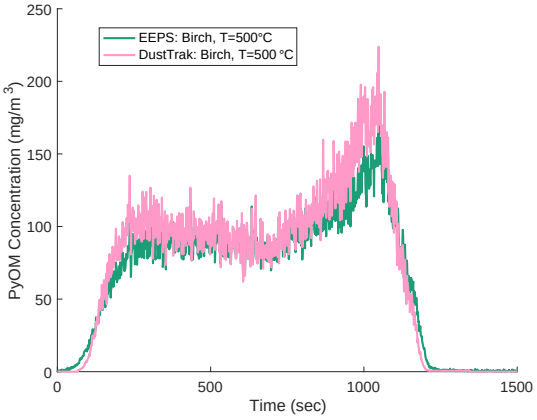

Figure S17. PyOM real-time concentration at 500°C as measured by the EEPS and DustTrak

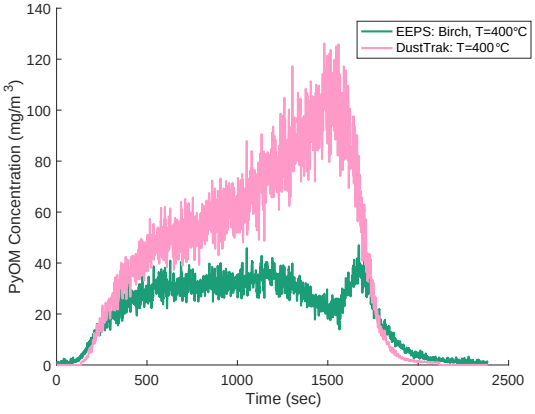

Figure S18. PyOM real-time concentration at 400°C as measured by the EEPS and DustTrak

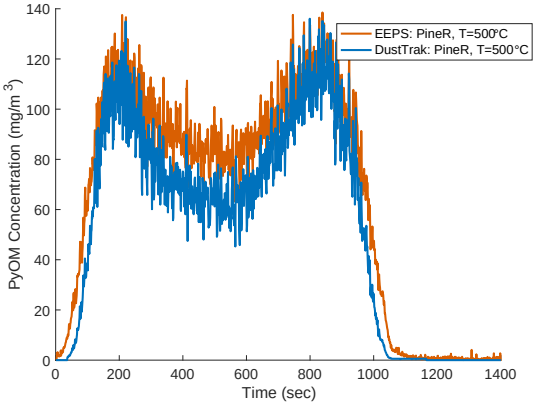

Figure S19. PyOM real-time concentration at 500°C as measured by the EEPS and DustTrak

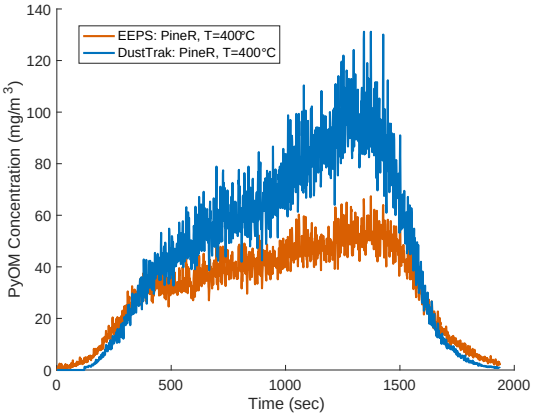

Figure S20. PPyOM real-time concentration at 400°C as measured by the EEPS and DustTrak

S4 Supporting Figures for Results Section

S4.1 Repeatability

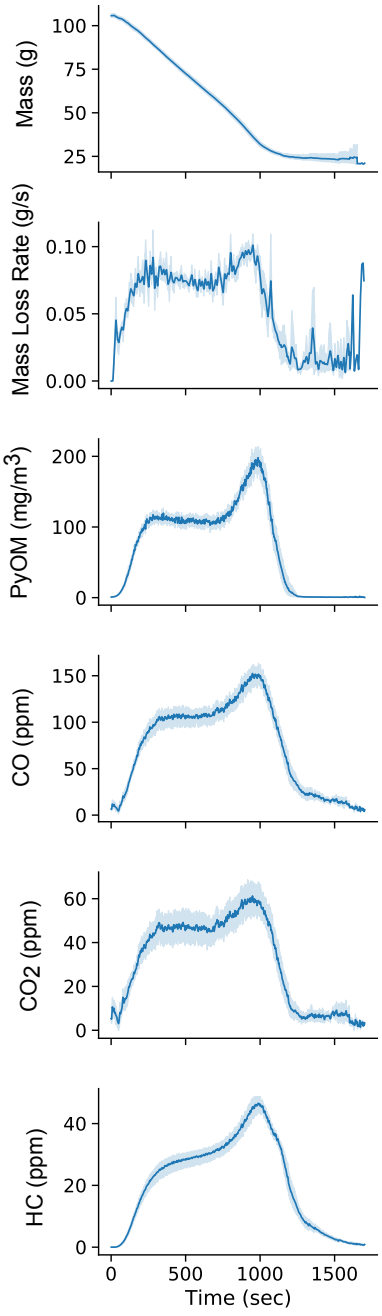

Figure S21. Repeatability of pyrolysis experiments for large birch at 500°C

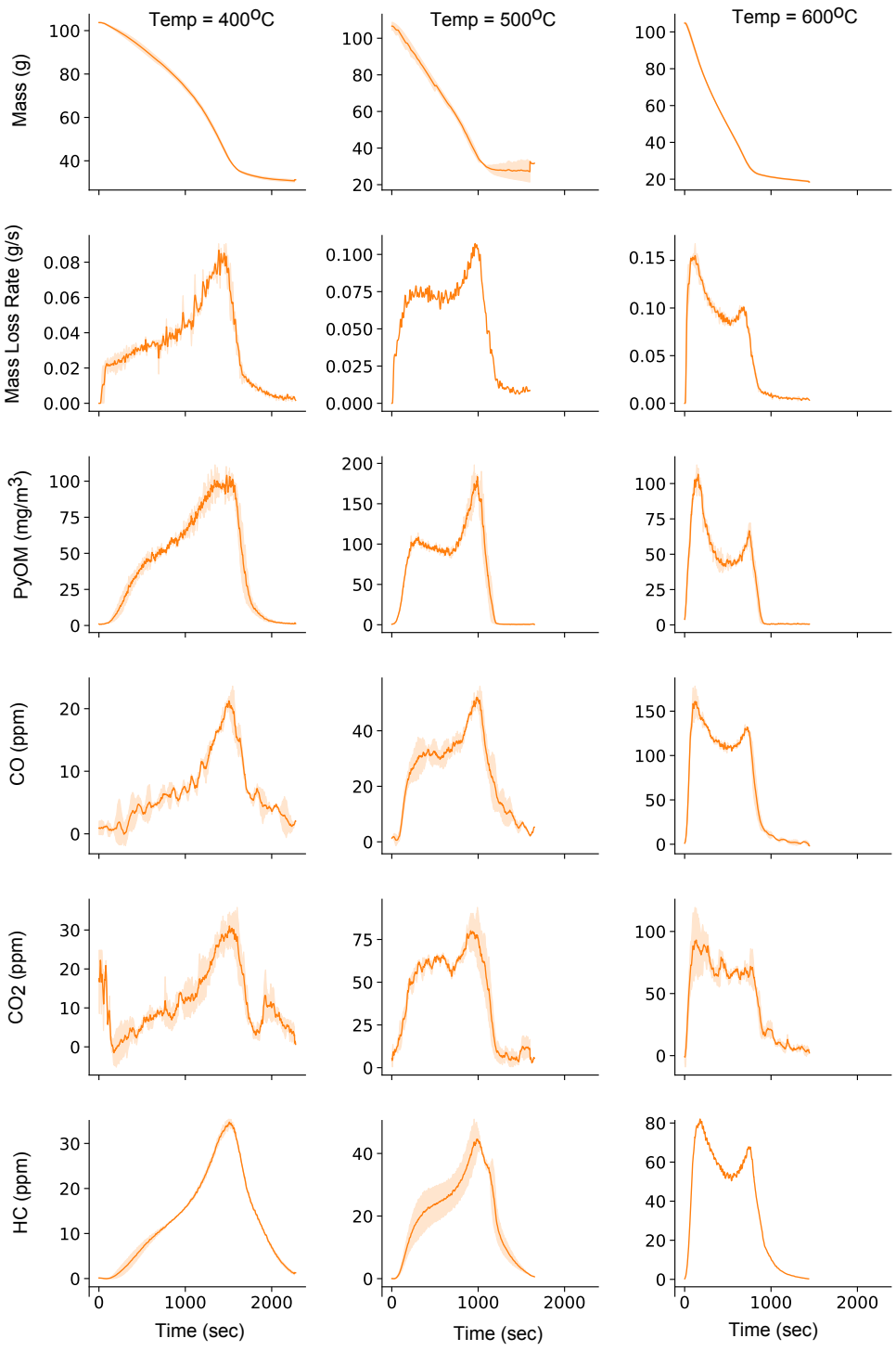

Figure S22. Mean and standard deviation of birch experiments at 400, 500, 600°C

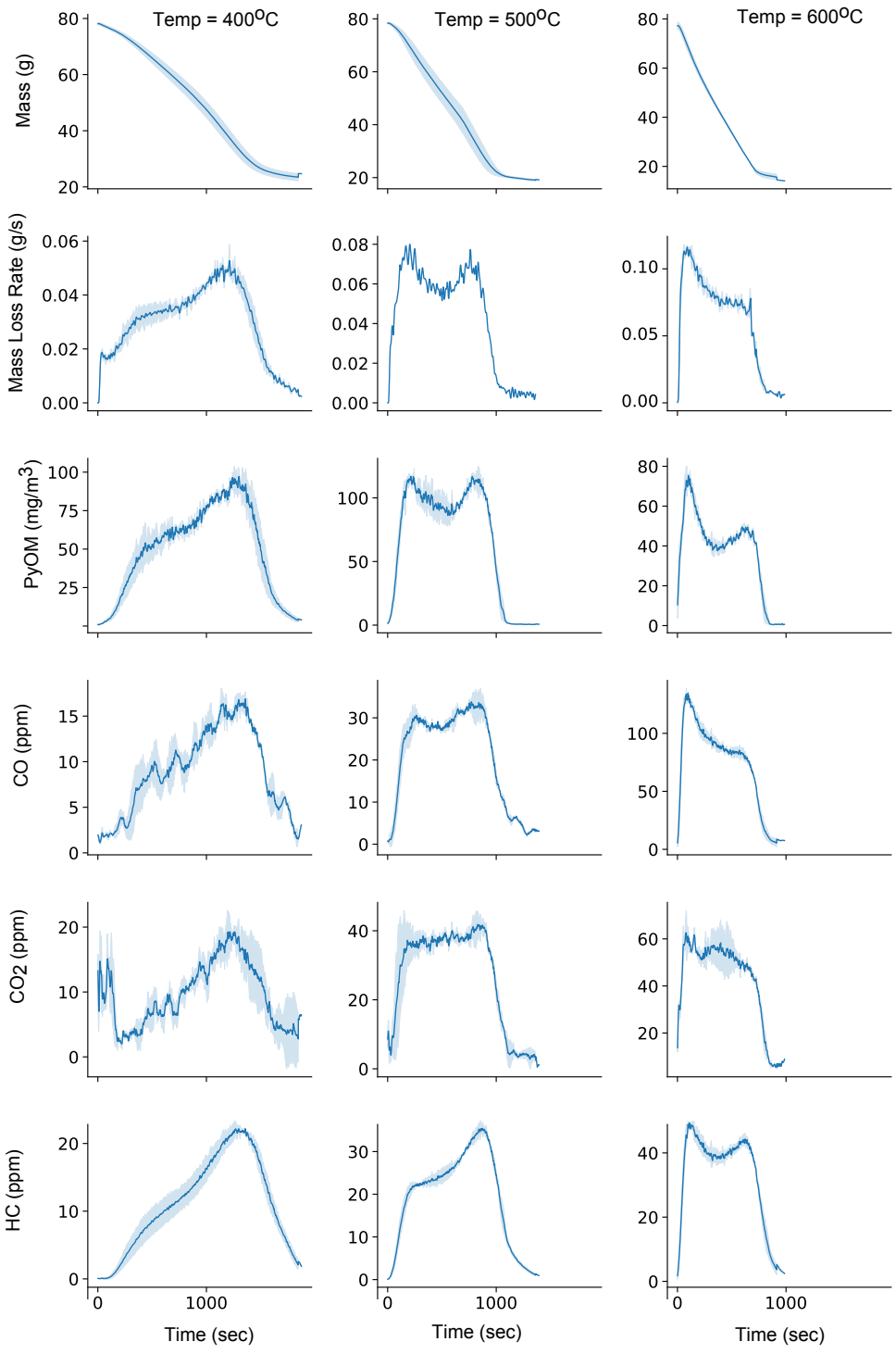

Figure S23. Mean and standard deviation of pineR experiments at 400, 500, 600°C

S4.2 Modified Combustion Efficiency

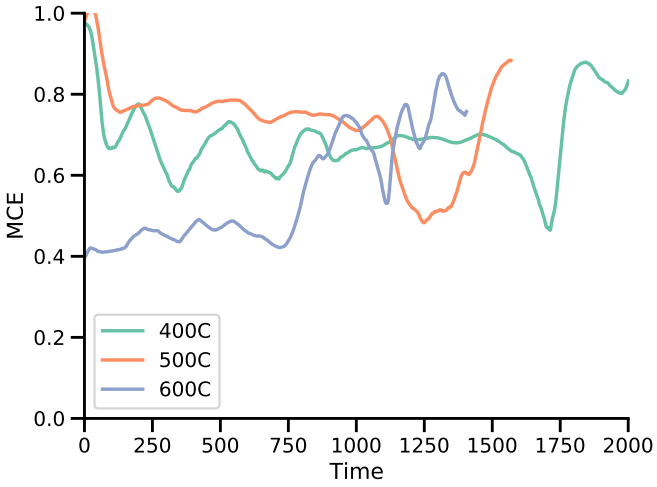

Figure S24. Modified combustion efficiency (MCE) of birch pyrolysis at the three reactor temperatures

S4.3 Gpyro Modeling

Using the modeling approach of Fawaz et al. (2020), we predict the mass loss rate of the pyrolysis of birch and pineR at 400, 500, and 600°C. Figures S25, S26, and S27 shows the prediction for pineR, and Figures S28, S29, and S30 show the prediction for birch.

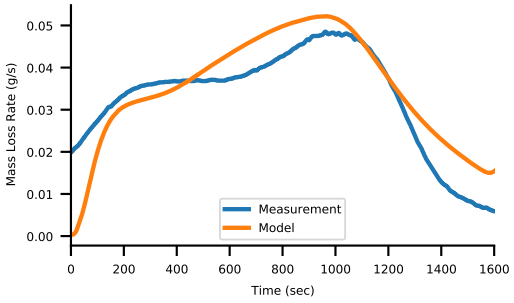

Figure S25. Gpyro modeling of mass loss rate of pineR pyrolysis at 400°C

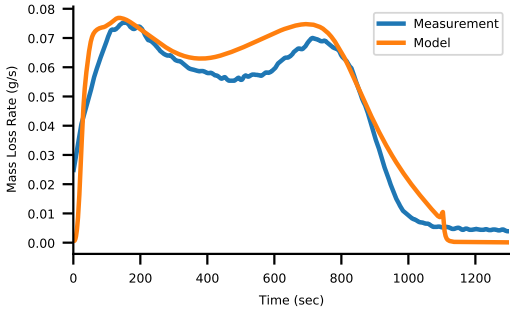

Figure S26. Gpyro modeling of mass loss rate of pineR pyrolysis at 500°C

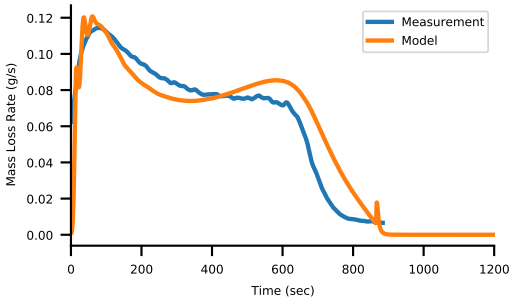

Figure S27. Gpyro modeling of mass loss rate of pineR pyrolysis at 600°C

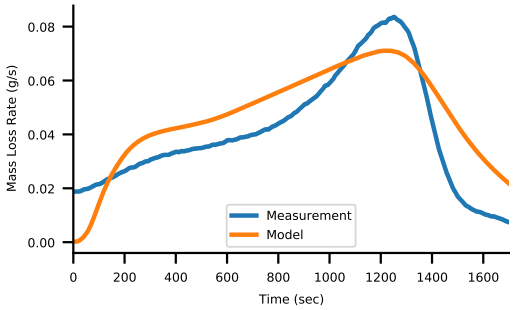

Figure S28. Gpyro modeling of mass loss rate of birch pyrolysis at 400600°C

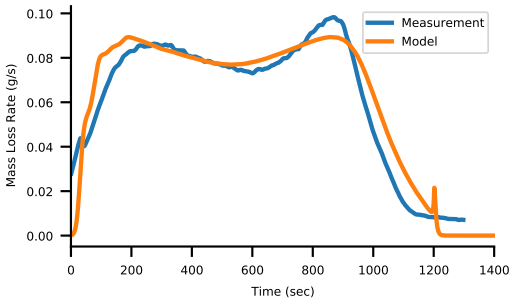

Figure S29. Gpyro modeling of mass loss rate of birch pyrolysis at 500°C

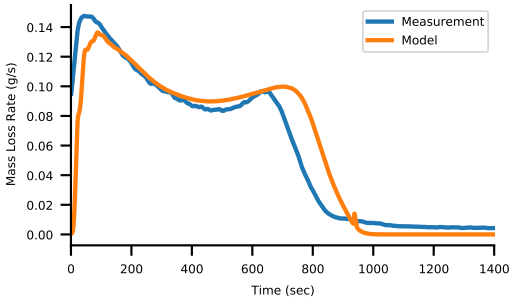

Figure S30. Gpyro modeling of mass loss rate of birch pyrolysis at 600°C

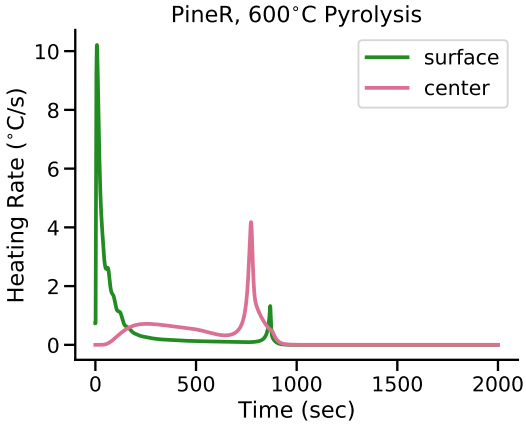

Figure S31. Gpyro modeling of heating rate of pineR pyrolysis at 600°C

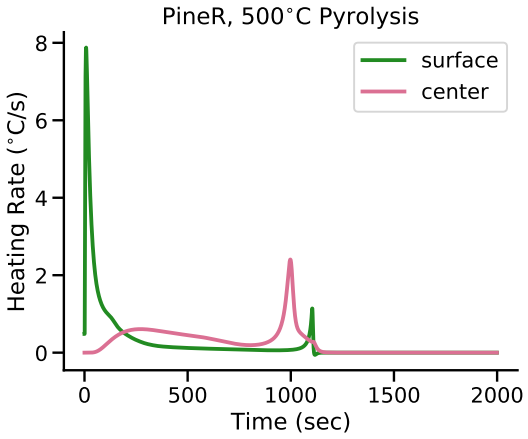

Figure S32. Gpyro modeling of heating rate of pineR pyrolysis at 500°C

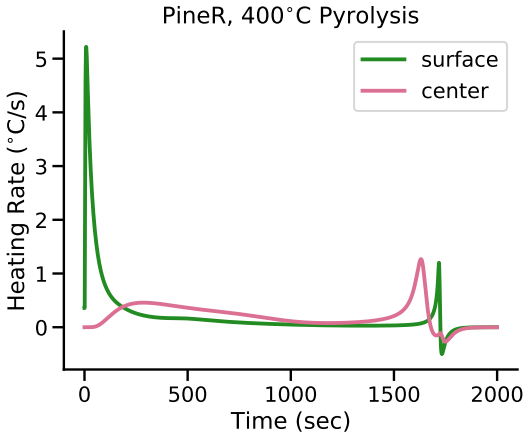

Figure S33. Gpyro modeling of heating rate of pineR pyrolysis at 400°C

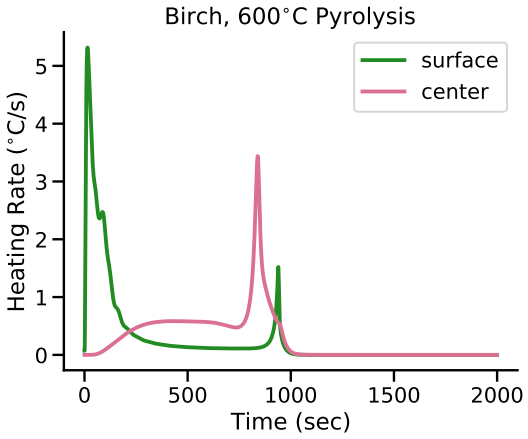

Figure S34. Gpyro modeling of heating rate of birch pyrolysis at 600°C

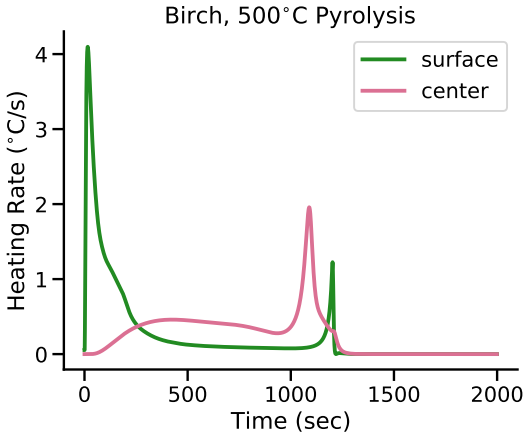

Figure S35. Gpyro modeling of heating rate of birch pyrolysis at 500°C

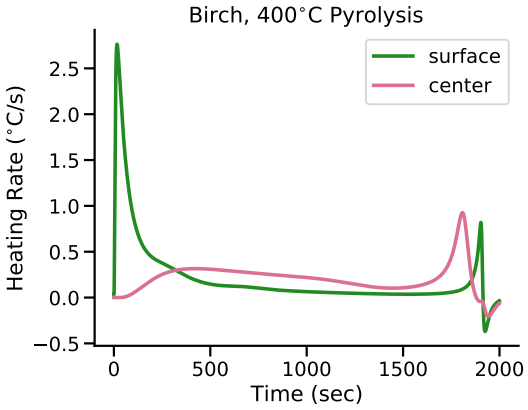

Figure S36. Gpyro modeling of heating rate of birch pyrolysis at 400°C

S4.4 Wood Size Figures

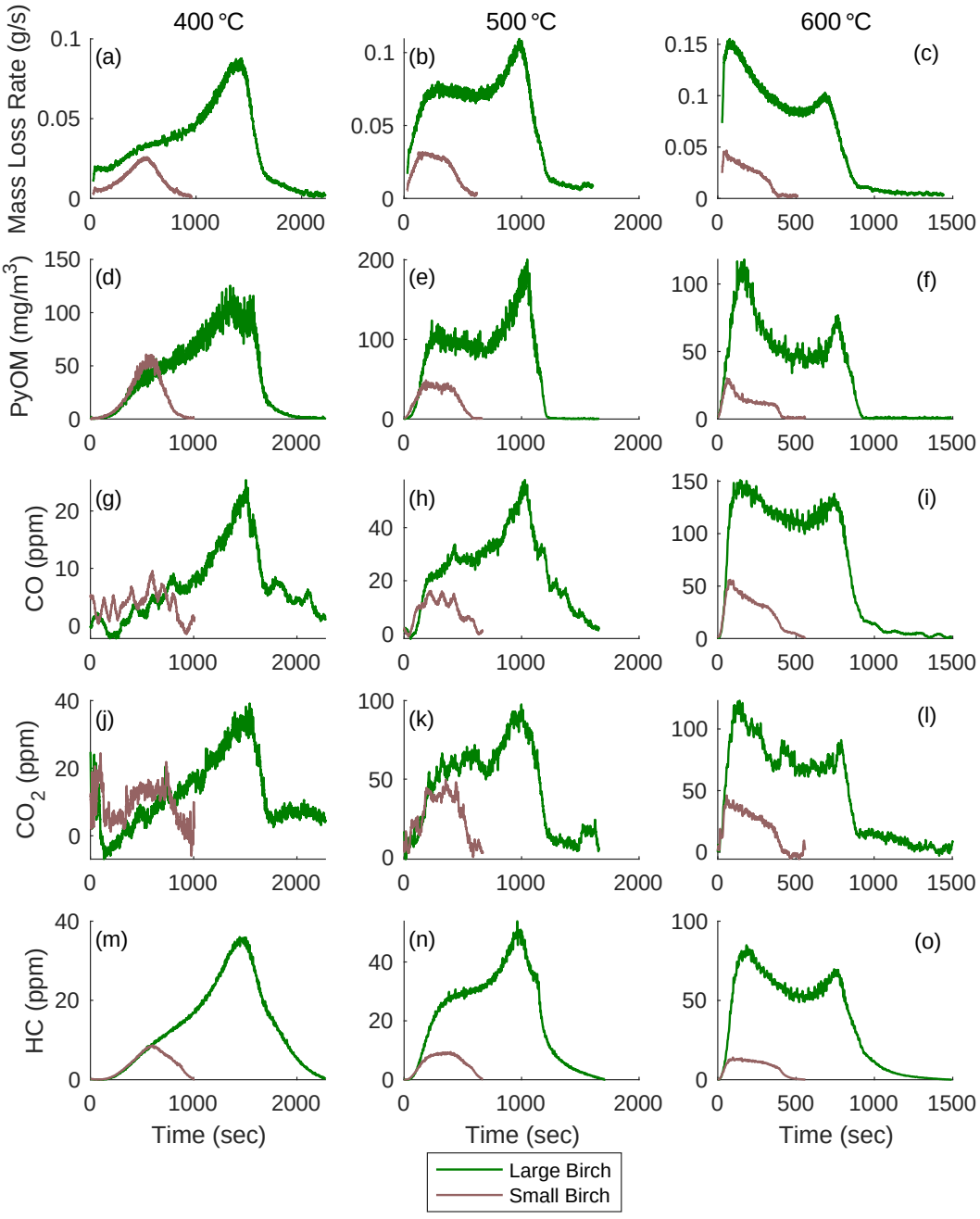

Figure S37. Real-time behavior of the pyrolysis of small and large birch wood

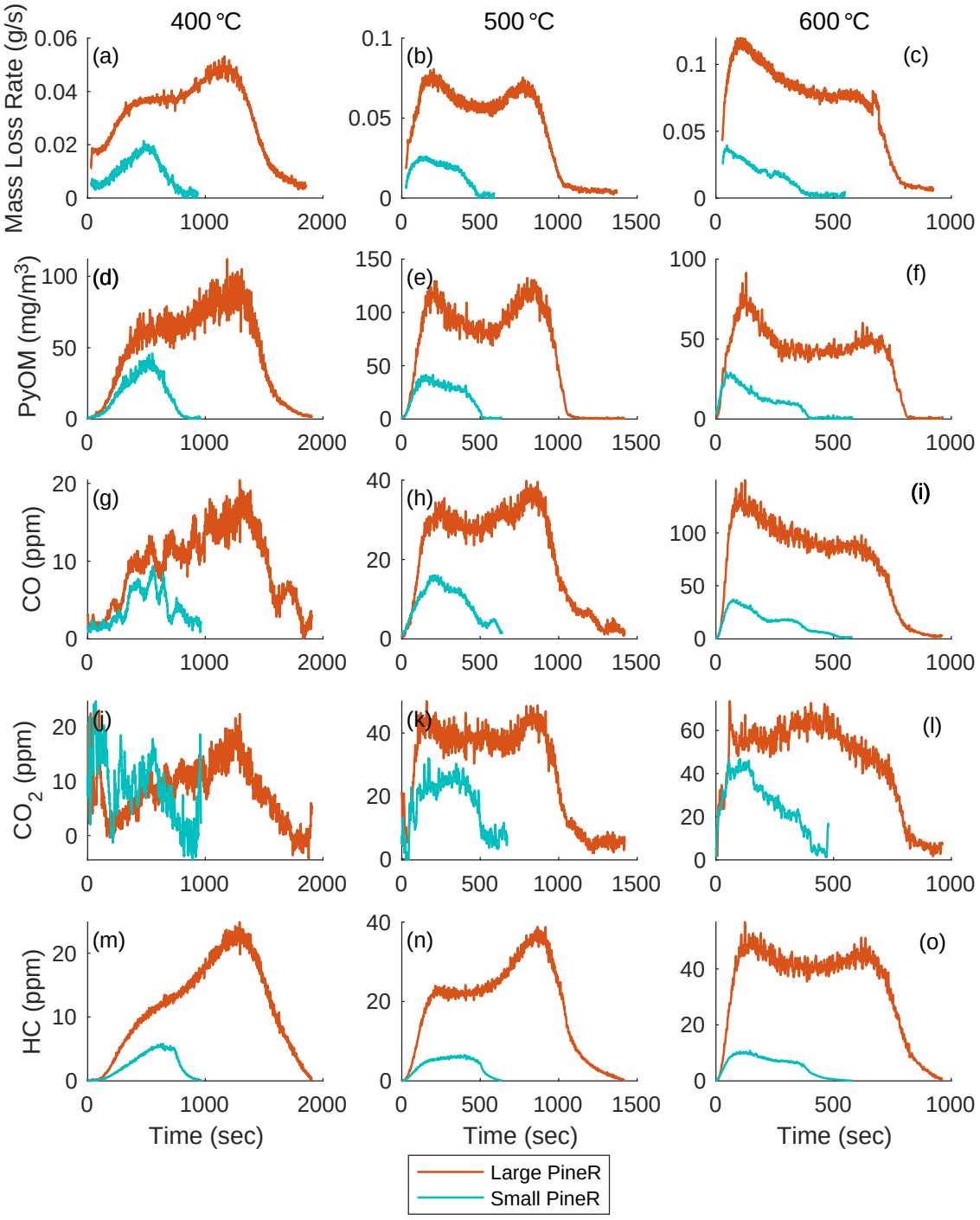

Figure S38. Real-time behavior of the pyrolysis of small and large pineR wood

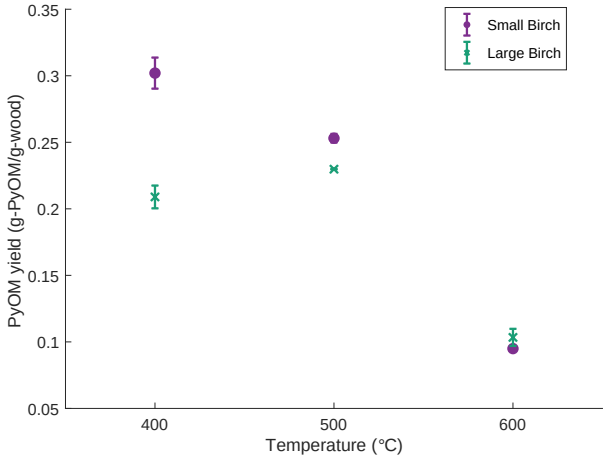

Figure S39. Comparison between the yields PyOM for small and large birch at the three reactor temperatures

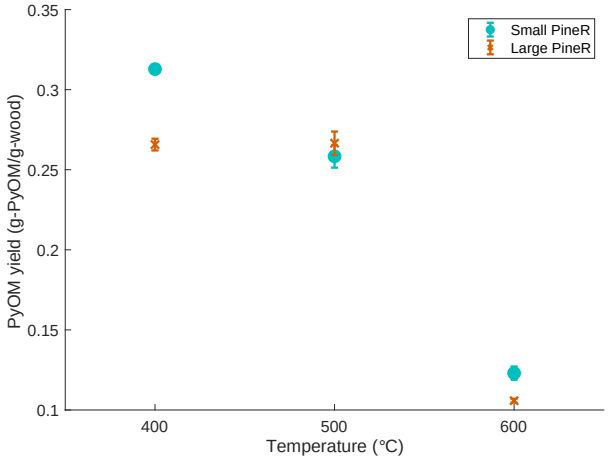

Figure S40. Comparison between the yields PyOM for small and large pineR at the three reactor temperatures

References

DeCarlo, P. F., Slowik, J. G., Worsnop, D. R., Davidovits, P., and Jimenez, J. L.: Particle morphology and density characterization by combined mobility and aerodynamic diameter measurements. Part 1: Theory, Aerosol Science and Technology, 38, 1185–1205, 2004.

Fawaz, M., Lautenberger, C., and Bond, T. C.: Prediction of organic aerosol precursor emission from the pyrolysis of thermally thick wood, Fuel, 269, 117 333, https://doi.org/10.1016/j.fuel.2020.117333, 2020.

Jayne, J. T., Leard, D. C., Zhang, X., Davidovits, P., Smith, K. A., Kolb, C. E., and Worsnop, D. R.: Development of an aerosol mass spectrometer for size and composition analysis of submicron particles, Aerosol Science & Technology, 33, 49–70, 2000.

Lee, B. P., Li, Y. J., Flagan, R. C., Lo, C., and Chan, C. K.: Sizing Characterization of the Fast-Mobility Particle Sizer (FMPS) Against SMPS and HR-ToF-AMS, Aerosol Sci. Tech., 47, 1030–1037, https://doi.org/10.1080/02786826.2013.810809, 2013.

Levin, M., Gudmundsson, A., Pagels, J. H., Fierz, M., Mølhave, K., Löndahl, J., Jensen, K. A., and Koponen, I. K.: Limitations in the Use of Unipolar Charging for Electrical Mobility Sizing Instruments: A Study of the Fast Mobility Particle Sizer, Aerosol Sci. Tech., 49, 556–565, https://doi.org/10.1080/02786826.2015.1052039, 2015.

Liu, P. S. K., Deng, R., Smith, K. A., Williams, L. R., Jayne, J. T., Canagaratna, M. R., Moore, K., Onasch, T. B., Worsnop, D. R., and Deshler, T.: Transmission Efficiency of an Aerodynamic Focusing Lens System: Comparison of Model Calculations and Laboratory Measurements for the Aerodyne Aerosol Mass Spectrometer, Aerosol Sci. Tech., 41, 721–733, https://doi.org/10.1080/02786820701422278, 2007.

Wang, X., Grose, M. A., Avenido, A., Stolzenburg, M. R., Caldow, R., Osmondson, B. L., Chow, J. C., and Watson, J. G.: Improvement of Engine Exhaust Particle Sizer (EEPS) size distribution measurement – I. Algorithm and applications to compact-shape particles, J. Aerosol Sci., 92, 95–108, https://doi.org/10.1016/J.JAEROSCI.2015.11.002, 2016.

Zimmerman, N., Godri Pollitt, K. J., Jeong, C.-H., Wang, J. M., Jung, T., Cooper, J. M., Wallace, J. S., and Evans, G. J.: Comparison of three nanoparticle sizing instruments: The influence of particle morphology, Atmos. Environ., 86, 140–147, https://doi.org/10.1016/J.ATMOSENV.2013.12.023, 2014.

Zimmerman, N., Jeong, C.-H., Wang, J. M., Ramos, M., Wallace, J. S., and Evans, G. J.: A source-independent empirical correction procedure for the fast mobility and engine exhaust particle sizers, Atmos. Environ., 100, 178–184, https://doi.org/10.1016/J.ATMOSENV.2014.10.054, 2015.